IEEE Access
Multidisciplinary ⋮ Rapid Review ⋮ Open Access Journal

Received 7 November 2022, accepted 16 November 2022, date of publication 21 November 2022, date of current version 7 December 2022.

*Digital Object Identifier 10.1109/ACCESS.2022.3224013*

RESEARCH ARTICLE

# Scattering Characteristics of an Electrically-Large Aircraft Object Illuminated by Bessel Vortex Beams

**ZHE WU[1], JIAJI WU[1], TAN QU[1], ZHENSEN WU[2], (Senior Member, IEEE), QIANG XU[2], HAIYING LI[2], LIN YANG[1], XIANGSHUAI MENG[3], AND JING BAI[4]**

[1]School of Electronic Engineering, Xidian University, Xi'an 710071, China
[2]School of Physics, Xidian University, Xi'an 710071, China
[3]School of Information and Communications Engineering, Xi'an Jiaotong University, Xi'an 710049, China
[4]School of Electronic Engineering, Xi'an University of Posts and Telecommunications, Xi'an, Shaanxi 710121, China

Corresponding authors: Jiaji Wu (wujj@mail.xidian.edu.cn) and Tan Qu (tqu@xidian.edu.cn)

This work was supported in part by the National Natural Science Foundation of China under Grant 62271381, Grant 62071359, Grant 62171355, Grant 61975158, Grant 62101426, and Grant 62001377; in part by the Open Project Foundation of Laboratory of Pinghu, Pinghu, China; in part by the China Postdoctoral Science Foundation under Grant 2020M683482; in part by the Natural Science Basic Research Plan in Shaanxi Province of China under Grant 2020JM-192; and in part by the Technology Foundation Strengthening Plan under Grant 2021-JCJQ-JJ-1009.

**ABSTRACT** Based on the excellent and broad prospect of the vortex beams in military application, it is necessary to evaluate the scattering characteristics of classical Bessel beam upon a perfect electrical conductor (PEC) blunt cone model of aircraft structure. First, a Bessel beam is expanded by a series of plane wave spectra. Then, combining the physical optics (PO) method, the scattered field of the object fitted by facet elements can be calculated. The amplitude, phase, and orbital angular momentum (OAM) spectra of scattered field for different object attitudes are discussed in detail. The results show that the backward scattering still retains good OAM characteristics, and which are distorted with the increase of oblique angle. Besides, the backscattering radar cross section (BRCS) of aircraft are also calculated and analyzed, and the scattered results of degenerated zero-order Bessel beam and plane wave are compared to verify the correctness of the proposed theory. Compared with plane waves, object scattering of vortex beams provides a new degree of freedom, providing more information for object detection.

**INDEX TERMS** Orbital angular momentum (OAM), physical optics (PO), plane wave spectra, aircraft, backscattering radar cross section (BRCS).

## I. INTRODUCTION

In recent years, vortex wave [1] has attracted more and more attentions because of its huge information carrying capacity and potential advantage in wireless communication system [2], [3]. In addition, vortex waves are also applied in radar imaging [4], [5], [6] and rotational Doppler detection [7]. At the same time, there are many reported approaches to generate vortex waves [8], [9], [10]. For circularly polarized (CP) incidence, the co- and cross-polarized output fields can be implemented functionalities separately to construct phase-modulated metasurfaces[11] for generating the vortex wave. By introducing detour phase[12], the design of the dual-polarized vortex beam generators in metasurface and metagrating form was proposed. In order to realize the application of vortex wave in object recognition and radar detection as soon as possible, the interaction mechanism between vortex wave and object is urgently needed.

According to our investigation, most of the object scattering characteristics of vortex waves are concentrated in the optical band. In particular, some results are obtained by using the wave function expansion method for microparticle spherical objects [13], [14], [15], [16], [17]. In [13], the scattering of light beam with OAM is studied by the Mie

The associate editor coordinating the review of this manuscript and approving it for publication was Mohammed Bait-Suwailam.

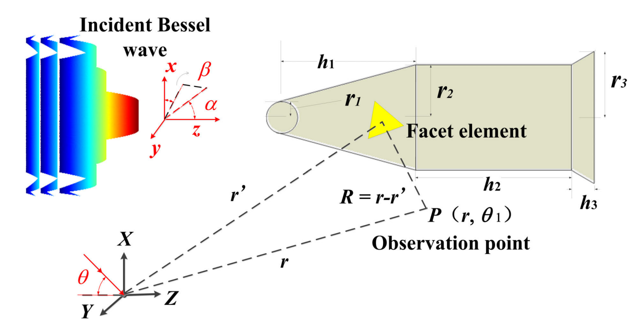


**FIGURE 1.** Geometric diagram of blunt cone aircraft. $h_1 = 4.965$ m, $h_2 = 4.5$ m, $h_3 = 0.6875$ m, $r_1 = 0.375$ m, $r_2 = 1$ m, $r_3 = 0.175$ m.

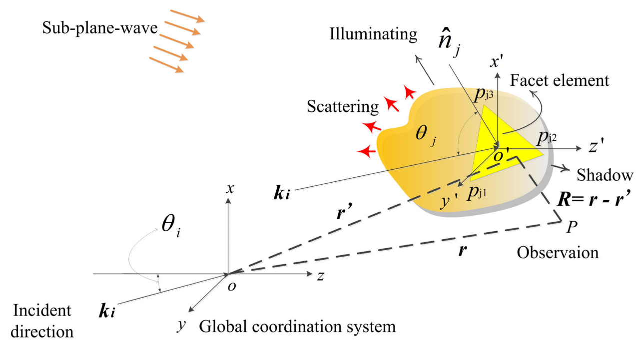


**FIGURE 2.** General convex object scatterers and parameter relations.

scattering theory. In [14], By utilizing the spherical harmonics partial wave series, the off-axial scattering of a Bessel beam by a rigid fixed sphere is presented. Besides, a FDTD solution [18] was used to realize the scattering characteristics of laser vortex beam by dielectric particles.

However, there are few studies on the interaction between vortex waves and electrically-large objects in microwave band. The high order Bessel vortex wave is scattered by several typical targets has been investigated by using the surface integral equation method [19]. The RCS and 3D directivity plots of the far-field scattering for a typical aircraft model were presented. A modified multilevel fast multipole algorithm (MLFMA) is presented [20] to analyze the OAM scattering from the electrically large object illuminated by a spiral parabolic antenna.

In [21], The backscattering of single and double spherical objects is obtained by experimental RCS measurement method. Following, the reflection and refraction of vortex waves on a flat plate are analyzed [22], whose result is not only from experiments but also from the spectral domain expansion theory. In [23], the vortex wave generated by the uniform circular array (UCA) irradiates the PEC sphere and PEC cone, and the backscattering is calculated by combining the Stratton-Chu equation. Regrettably, the above reports are limited to solving the simple object scattering. For arbitrary convex objects, there is a lack of a comprehensive and systematic scattering calculation method.

In this paper, we calculate the vortex scattering of a scale model for aircraft structure named 'raging fire'. In order to calculate scattering by PO algorithm, the object is divided into a series of fitting triangular facet elements. For each element, the amplitude, phase, and polarization of incident Bessel beam is different. Therefore, Bessel beam should not be directly brought into PO integral for calculation. Consequently, the Bessel beam is expanded into a superposition of a series of plane waves, and PO is performed to each sub-plane-wave. Finally, the scattering of all decomposed sub-plane-wave on all facet elements are summed vectorially to obtain the final result.

## II. CALCULATION METHOD

As illustrated in Fig. 1, a Bessel beam propagating along the $+z$ axis illuminates an aircraft structure. The coordinate system of incident Bessel beam is represented by the $o$-$xyz$, and the o in the global coordinate system O-XYZ are $(x_0, y_0, z_0)$. The time harmonic factor $\exp(-i\omega t)$ is assumed for convenience.

### A. INCIDENT BESSEL BEAM

Based on the vector angular spectrum decomposition (VASD), the incident electric field of Bessel beam at $(x_0, y_0, z_0)$ can be expressed as [16]

$$\vec{E}^{inc}(x, y, z) = k^2 \int_{\beta=0}^{2\pi} \int_{0}^{\pi/2} \vec{A}(\alpha, \beta) \exp(ikr \sin\alpha \sin\theta \cos(\beta - \phi)) \times \exp(ikr \cos\alpha \cos\theta) \exp(-kz_0 \cos\alpha) \sin\alpha \cos\alpha d\alpha d\beta \tag{1}$$

where $\vec{A}(\alpha, \beta) = A(\alpha, \beta)\vec{f}(\alpha, \beta)$, $A(\alpha, \beta)$ and $f(\alpha, \beta)$ are the scalar amplitude and polarization state respectively. The angles $\alpha$ and $\beta$ are defined as the elevation and azimuth angles in the beam coordination system.

$$\vec{f}(\alpha, \beta) = a\vec{e}_x + b\vec{e}_y - (\frac{\sin\alpha \cos\beta}{\cos\alpha} a + \frac{\sin\alpha \sin\beta}{\cos\alpha} b)\vec{e}_z \tag{2}$$

In this paper, the Bessel beam is selected as examples to conduct the analysis. The scalar amplitude function of a Bessel beam with arbitrary integer order is

$$A(\alpha, \beta) = \frac{\delta(\alpha - \alpha_0)}{\sin\alpha_0} e^{il\beta} \tag{3}$$

where the parameter $\delta$ represents the Dirac function, $l$ denotes the integer order topological charge, and $\alpha_0$ is the half-cone angle.

### B. PO METHOD

Fig. 2 shows the model diagram of the general convex object fitted by a series of facet elements under the irradiation of the decomposed sub-plane-wave. According to the Stratton-Chu equation, the scattered field at an external position of any triangular facet element *j-th* on the PEC scatters can be given

$$\vec{E}_j^s = \frac{i}{\omega\varepsilon \cdot 4\pi} \int_{s'} [\frac{3 - k^2R^2 - i3kR}{R^5} e^{ikR} \vec{R} \times (\vec{R} \times \vec{J}_s(r')) + 2\vec{J}_s(r') \frac{1 - ikR}{R^3} e^{ikR}] ds' \tag{4}$$

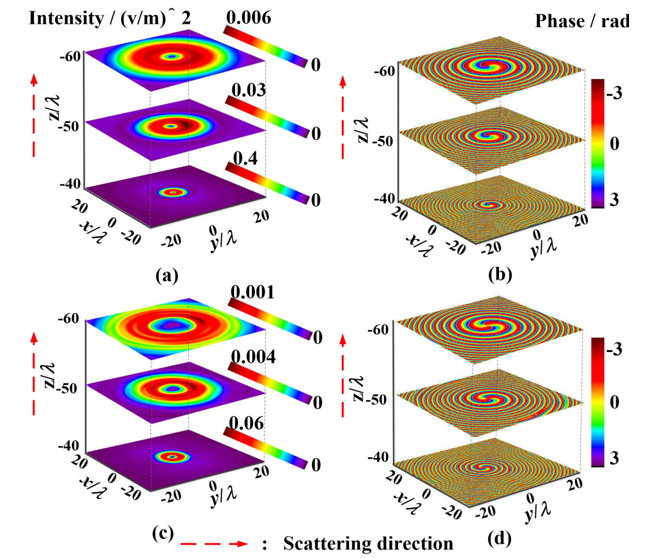


**FIGURE 3.** Intensity and phase distributions of the backward scattered electric field (x component). (a) Intensity (l=1); (b) Phase (l=1); (c) Intensity (l=2); (d) Phase (l=2).

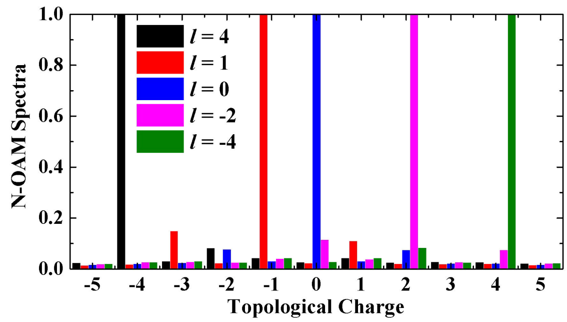


**FIGURE 4.** Normalized OAM spectra of the backward scattered field with different topological charge.

where

$$\begin{cases} \vec{J}_s(r') = \begin{cases} 2\hat{n}_j \times \vec{H}_j^i, & \text{illuminated regions} \\ 0, & \text{others} \end{cases} \\ \hat{n}_j \times \vec{H}_j^i = \dfrac{1}{\eta}\left[E_\perp^i \cos\theta_i \hat{e}_\perp^j + E_\parallel^i (\hat{n} \times \hat{e}_\perp^j)\right] \end{cases} \tag{5}$$

$$\hat{e}_{1j} = \frac{\hat{e}_{2j} \times \vec{k}_i'}{\left|\hat{e}_{2j} \times \vec{k}_i'\right|}, \quad \hat{e}_{2j} = \frac{\vec{k}_i' \times \hat{n}_j}{\left|\vec{k}_i' \times \hat{n}_j\right|} \tag{6}$$

and $E_\perp^{ij}(r) = \hat{e}_\perp^j \cdot \vec{E}_j^i(r)$ and $E_\parallel^{ij}(r) = \hat{e}_\parallel^j \cdot \vec{E}_j^i(r)$ denote the incident electric field components on triangular facet element $j$-$th$ in the directions of perpendicular polarization $\hat{e}_\perp^j$ and parallel polarization $\hat{e}_\parallel^j$. $\vec{E}_j^i(r)$ is the any exploded sub-plane-wave of incident electric field in (1). $\hat{n}_j$ is the normal unit vector of the facet element $j$-$th$ on object. $\theta_i$ is the incident direction of each decomposed plane wave angular spectrum. Taking into account the transformation relationship of coordinate systems, substituting (1) and (5) into (4) and switching the order of integral operation can obtain the scattered field.

$$\vec{E}_{total}^s = k^2 \iint \sum_{j=1}^{N_e} \vec{E}_j^s \sin\alpha \cos\alpha d\alpha d\beta \tag{7}$$

where $N_e$ is the number of partitioned surface elements.

Finally, the far-field RCS of the Bessel beam can be defined as

$$RCS = \lim_{R\to\infty} 4\pi R^2 \frac{\left|\vec{E}_{total}^s\right|^2}{\left|\vec{E}^{inc}\right|^2} \tag{8}$$

## III. RESULTS AND ANALYSIS

In this section, numeric calculations are conducted to analyze and evaluate the backward scattered field and BRCS for aircraft object that is divided into 20002 triangular facet elements with side length of 0.3λ (λ is 300mm). Assuming that the $x$-polarized Bessel beam ($a = 1, b = 0$) is incident in the head of the aircraft, the observation cross section is $40\lambda \times 40\lambda$, and the tail of the aircraft coincides with $z = 0$ plane.

### A. BACKWARD SCATTERING RESULT

Fig. 3 depicts the amplitude and phase cross section distributions of the backward scattering varying with the scattering distance. This clearly shows that the backward scattered field still maintains good OAM characteristic maybe due to the symmetrical object. In the cases of both topological charge $l = 1$ and $l = 2$, amplitude hollow and helical phase wavefront characteristics are presented, and the Bessel wave can generate diffusion and attenuation as the scattering distance increases. In addition, compared with $l = 1$, the amplitude hollow becomes larger and the magnitude decreases in the case of $l = 2$, which is consistent with the characteristics of incident Bessel beam.

In order to further analyze the OAM modal purity of the back echo, Fig. 4 presents the normalized scattered OAM spectra distributions under the incident Bessel beam with different topological charge. It can be seen that all scattering OAM spectra obtain a high modal distribution under the different topological charges, and the maximum percentage of hybrid modes is less than 15% ($l = 1$). This shows that for a blunt cone aircraft object with symmetric prototype, the backward scattered field has a good OAM characteristics similar to the incident field when the normal incidence occurs. Besides, the topological charge of the Bessel echo is the negative value of the topological charge of incident Bessel beam.

Further, the backward scattered amplitude and phase distributions under different degrees of deviation from the vertical incident direction are illustrated in Fig. 5. The relative position relationships are indicated in the diagram. With the increase of oblique incidence angle, the backward scattered Bessel wave will produce some distortion, which is manifested in the gradual loss of hollow amplitude and spiral phase wavefront respectively. When the oblique angle is

 

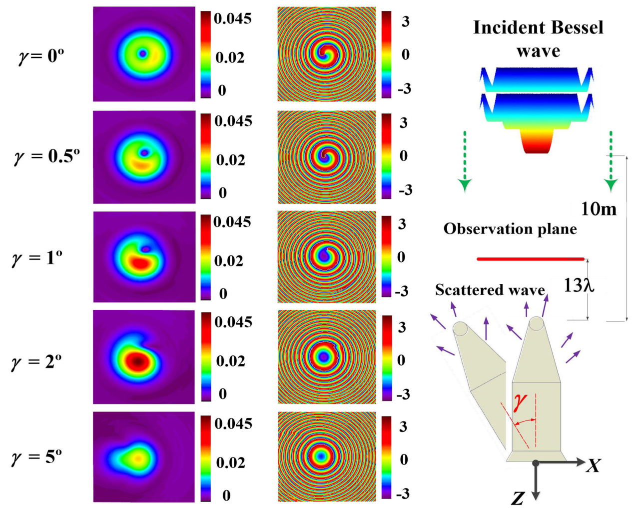


**FIGURE 5.** Variation of the amplitude and phase distributions (40λ × 40λ) with different title angle.

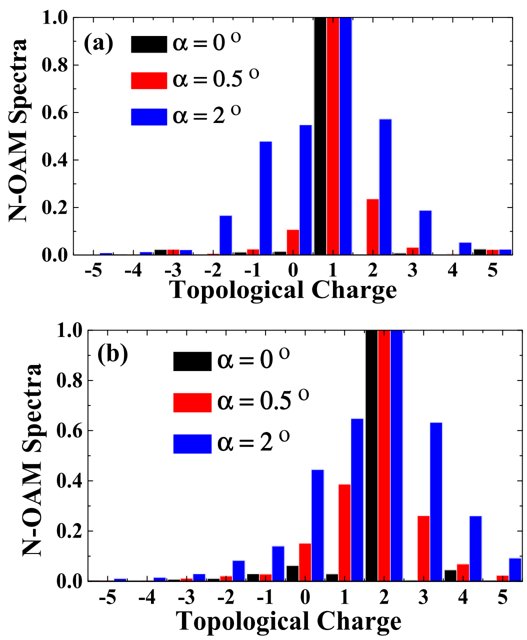


**FIGURE 6.** Normalized OAM spectra of scattered field with different tilted angle. (a), ($l = -1$); (b), ($l = -2$).

less than 1°, the phase distribution is still helical while the amplitude has lost the circular distribution. When the oblique angle exceeds 2°, the Bessel wave loses the helical phase wavefront and the amplitude distribution becomes conical shape gradually.

Finally, Fig. 6 shows the normalized OAM spectra distributions at different tilt angles $\alpha$. The proportion of the hybrid modes is enhanced with the increase of the tilt angle, which corresponds to the distortion of the backward Bessel scattered waves. Regardless of $l = 1$ or 2, the highest proportion of the hybrid mode reaches about 60% when the oblique incidence angle is 2°, which is mutually confirmed with the

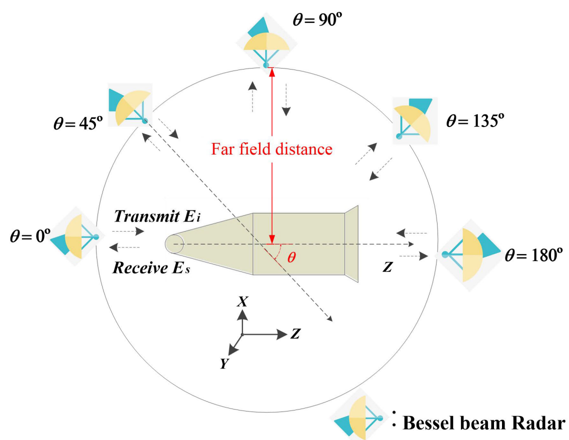


**FIGURE 7.** Schematic diagram of the backscattering case of Bessel beam radar.

loss of OAM characteristics of the scattered field under the corresponding case in Fig. 5.

### B. BRCS OF THE AIRCRAFT

In this section, the backscattering characteristics of aircraft are mainly discussed. Fig. 7 is a schematic diagram of the aircraft's backscattering of Bessel radar. The Bessel radar scans clockwise from the head ($\theta = 0°$) to the tail ($\theta = 180°$) of the aircraft. Similarly, the far-region scattered field of a PEC object can be obtained by PO integral as follows

$$E^s = -\frac{ik^2}{2\pi\omega\mu}\frac{\exp(ikr)}{r}\int_{s1}\hat{R}\times[\hat{R}\times(\hat{n}\times H^i)] \times \exp(-ik\hat{R}\cdot r')ds' \quad (9)$$

where the incident field is in the opposite direction to that of the scattered field.

To verify the correctness of aircraft scattering calculated by the proposed method for Bessel wave, the object is illuminated by the degraded Bessel beam ($l = 0°, \alpha_0 = 0°$) and plane wave, respectively. As shown in Fig. 8, the peak value of BRCS of both the plane wave and the zero-order Bessel beam appear at the tail ($\theta = 180°$) direction, which can be interpreted as a circular planar structure with a high RCS at the tail. When $\theta = 90°$, The zero depth of BRCS occurs maybe due to the discontinuities between the cone and cylinder in this aircraft structure. The BRCS curves from the illumination of the above two types of incident wave coincide well, which effectively verifies the proposed theoretical method and program code. Some subtle differences may be due to the numerical algorithm errors and facet element precision.

Fig. 9 shows the BRCS curves of aircraft under Bessel beam irradiation with different topological charges and different half-cone angles. Fig. 9.(a) shows that the backscattering curves of Bessel beam with different topological charges have few differences. Compared with plane wave's irradiation, zero depth appear at both $\theta = 0°$ and $\theta = 180°$, which is

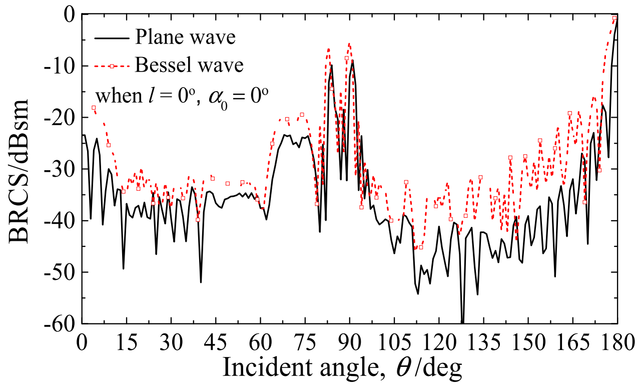


**FIGURE 8.** The BRCS comparisons of degraded Bessel wave ($l = 0°$, $\alpha_0 = 0°$) and plane wave.

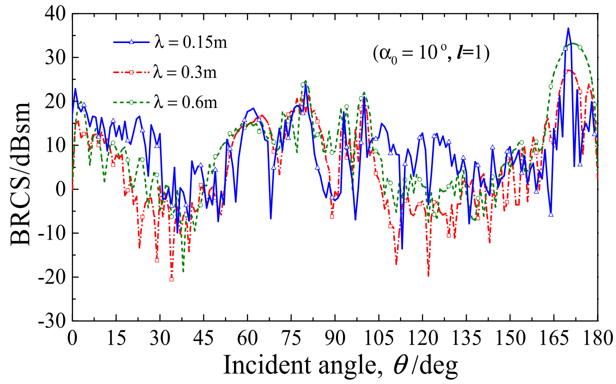


**FIGURE 10.** The BRCS results of Bessel beams with different incident wavelength.

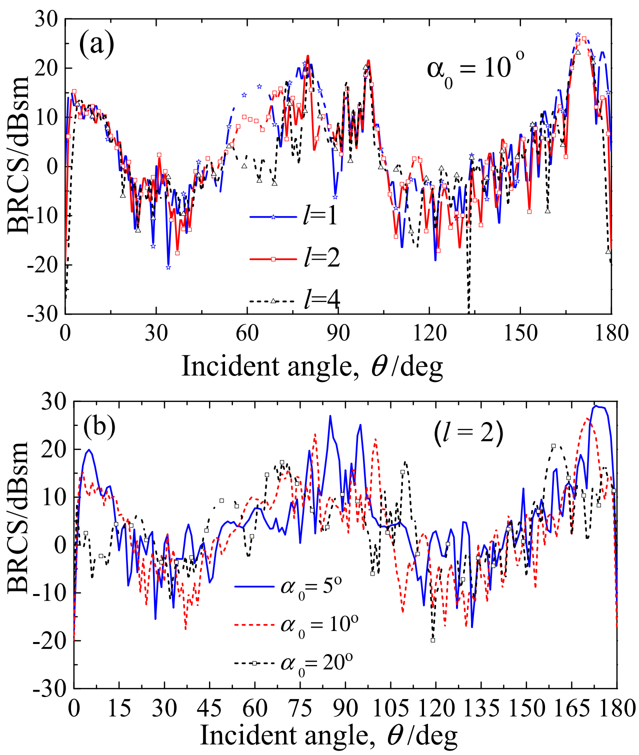


**FIGURE 9.** The BRCS results of Bessel beams with different topological charge (a) and different half-cone angle (b).

the most significant target characteristic difference between plane wave and Bessel wave. As can be seen from Fig. 9. (b), with the increase of the half-cone angle, the BRCS level of Bessel wave decreases, while the central deviation occurs at all the three strong scattering positions of $\theta = 0°$, $\theta = 90°$, and $\theta = 180°$. The BRCS variation of Bessel beam with different half-cone angle also provides an additional recognition information for the object, which further enhances the accuracy and reliability of object recognition.

Although the BRCS curves with different topological charges have few differences as shown in Fig. 9. (a), the fast Fourier transform (FFT) corresponding to different OAM states can obtain more abundant information in azimuth angle. Therefore, by using Bessel wave to replace plane wave in synthetic aperture radar (SAR) imaging algorithm, a good transverse resolution can be obtained [24]:

$$\rho_a = \lambda/2\theta_{BW} \tag{10}$$

where $\rho_a$ is the azimuth resolution, $\lambda$ is the wavelength, and $\theta_{BW}$ is the effective azimuth beam width. For circular array with the same antenna aperture size, vortex wave and ordinary electromagnetic wave can be generated respectively with or without phase delay. The azimuth beamwidth of the far field pattern of vortex wave is larger than that of traditional electromagnetic wave evidently. Therefore, higher azimuth resolution of OAM imaging can be obtained according to (9).

Fig. 10 presents the BRCS of Bessel beams with different incident wavelengths, and the result shows that the curve fluctuation becomes more obvious with the decrease of wavelength. Importantly, this numerical method has a strong universality and can be applied to the acquisition of electrically-large object characteristics in the terahertz or even optical frequency band.

## IV. CONCLUSION

This paper investigates the interaction mechanism between Bessel beam and a blunt cone aircraft object. The combination of angular spectra expansion and facet segmentation method makes the object scattering characteristic of Bessel waves not limited to simple structures. The distribution of backward scattered fields and OAM spectra obtained from different object attitudes reveal that the OAM characteristics of Bessel vortex wave echo from symmetric object are better than those from asymmetric object. The backscattering results show that the strong scattering points of the aircraft object include head, side and tail. There is no significant difference in the BRCS of Bessel beam with different topological charges. However, the BRCS phenomenon under different half-cone angle at the main scattering positions is similar to the characteristics of incident Bessel wave: with the increase of the half-cone angle, the amplitude decreases and the main lobe shifts away from the zero depth. This study has great potential significance for future military radar and Bessel vortex object recognition.

## ACKNOWLEDGMENT
The authors would like to thank the anonymous reviewers for their valuable comments and suggestions.

## REFERENCES
[1] L. Li, H. Xue, and Q. Feng, "Research progresses in theory and applications of vortex electromagnetic waves," *J. Microw.*, vol. 34, no. 2, pp. 1–12, 2018.
[2] W. Shao, S. Huang, X. Liu, and M. Chen, "Free-space optical communication with perfect optical vortex beams multiplexing," *Opt. Commun.*, vol. 427, pp. 545–550, Nov. 2018.
[3] Q. Chang, C. Lin, and X. X. Li, "Development and status of electromagnetic vortex communication technology," *Syst. Eng. Electron.*, vol. 40, no. 11, pp. 2554–2565, 2018.
[4] T. Yuan, H. Wang, Y. Cheng, and Y. Qin, "Electromagnetic vortex-based radar imaging using a single receiving antenna: Theory and experimental results," *Sensors*, vol. 17, no. 3, p. 630, Mar. 2017.
[5] T. Yang, W. Huang, and X. Lu, "Two dimensional forward-looking missile-borne radar imaging based on vortex electromagnetic waves," *IEEE Access*, vol. 8, pp. 221103–221110, 2020.
[6] X. X. Bu, Z. Zhang, L. Y. Chen, K. H. Zhu, S. Zhou, J.-P. Luo, R. Cheng, and X.-D. Liang, "Synthetic aperture radar interferometry based on vortex electromagnetic waves," *IEEE Access*, vol. 7, pp. 82693–82700, 2019.
[7] M. P. J. Lavery, F. C. Speirits, S. M. Barnett, and M. J. Padgett, "Detection of a spinning object using light's orbital angular momentum," *Science*, vol. 341, no. 6145, pp. 537–540, 2013.
[8] T. Yuan, Y. Cheng, H.-Q. Wang, and Y. Qin, "Generation of OAM radio beams with modified uniform circular array antenna," *Electron. Lett.*, vol. 52, no. 11, pp. 896–898, 2016.
[9] M. Lin, Y. Gao, P. Liu, and J. Liu, "Theoretical analyses and design of circular array to generate orbital angular momentum," *IEEE Trans. Antennas Propag.*, vol. 65, no. 7, pp. 3510–3519, Jul. 2017.
[10] Y. Huang, X. Li, Z. Akram, H. Zhu, and Z. Qi, "Generation of millimeter-wave nondiffracting airy OAM beam using a single-layer hexagonal lattice reflectarray," *IEEE Antennas Wireless Propag. Lett.*, vol. 20, no. 6, pp. 1093–1097, Jun. 2021.
[11] Y. Yuan, S. Sun, Y. Chen, K. Zhang, X. Ding, B. Ratni, Q. Wu, S. N. Burokur, and C. W. Qiu, "A fully phase-modulated metasurface as an energy-controllable circular polarization router," *Adv. Sci.*, vol. 7, no. 18, Sep. 2020, Art. no. 2001437.
[12] K. Zhang, Y. Wang, S. N. Burokur, and Q. Wu, "Generating dual-polarized vortex beam by detour phase: From phase gradient metasurfaces to metagratings," *IEEE Trans. Microw. Theory Techn.*, vol. 70, no. 1, pp. 200–209, Jan. 2022.
[13] P. Acharya and A. M. Guzmán, "Mie scattering of light with orbital angular momentum by nanoparticles," *Proc. SPIE, 22nd Congr. Int. Commission Opt., Light Develop. World*, vol. 8011, pp. 1–7, Oct. 2011, Art. no. 801145, doi: 10.1117/12.903437.
[14] F. G. Mitri and G. T. Silva, "Off-axial acoustic scattering of a high-order Bessel vortex beam by a rigid sphere," *Wave Motion*, vol. 48, no. 5, pp. 392–400, 2011.
[15] Q. Tan, W. Zhensen, W. Y. Yu, L. Zhengjun, and B. Lu, "Analysis of scattering characteristics of Laguerre Gaussian vortex beams to biological cells," *Acta Optica Sinica*, vol. 35, pp. 1–10, Jul. 2015.
[16] H. Tang, R. Li, S. Gong, B. Wei, L. Yang, Z. Zhu, Y. Wu, and F. G. Mitri, "Scattering of arbitrary-shaped optical polarized beams by a PEMC sphere," *J. Quant. Spectrosc. Radiat. Transf.*, vol. 281, Apr. 2022, Art. no. 108101.
[17] T. Qu, Z. S. Wu, Q. C. Shang, and Z. J. Li, "Light scattering of a Laguerre–Gaussian vortex beam by a chiral sphere," *J. Opt. Soc. Amer. A, Opt. Image Sci.*, vol. 33, no. 4, pp. 475–482, Apr. 2016.
[18] W. Sun, Y. Hu, C. Weimer, K. Ayers, R. R. Baize, and T. Lee, "A FDTD solution of scattering of laser beam with orbital angular momentum by dielectric particles: Far-field characteristics," *J. Quant. Spectrosc. Radiat. Transf.*, vol. 188, pp. 200–213, Feb. 2017.
[19] M. P. Yu, Y. Han, and Z. Cui, "Scattering of non-diffracting vortex electromagnetic wave by typical targets," *Prog. Electromagn. Res. Lett.*, vol. 70, pp. 139–146, 2017.
[20] B. H. Yin, Z. He, and R. S. Chen, "Propagating and scattering of the electromagnetic vortex generated by a spiral parabolic antenna," *Appl. Comput. Electromagn. Soc. J.*, vol. 34, no. 11, pp. 1637–1644, 2019.
[21] C. Zhang, D. Chen, and X. Jiang, "RCS diversity of electromagnetic wave carrying orbital angular momentum," *Sci. Rep.*, vol. 7, no. 1, p. 15412, Nov. 2017.
[22] Y. Yao, X. Liang, M. Zhu, W. Zhu, J. Geng, and R. Jin, "Analysis and experiments on reflection and refraction of orbital angular momentum waves," *IEEE Trans. Antennas Propag.*, vol. 67, no. 4, pp. 2085–2094, Apr. 2019.
[23] K. Liu, H. Liu, W. E. I. Sha, Y. Cheng, and H. Wang, "Backward scattering of electrically large standard objects illuminated by OAM beams," *IEEE Antennas Wireless Propag. Lett.*, vol. 19, no. 7, pp. 1167–1171, Jul. 2020.
[24] X. Bu, Z. Zhang, L. Chen, X. Liang, H. Tang, and X. Wang, "Implementation of vortex electromagnetic waves high-resolution synthetic aperture radar imaging," *IEEE Antennas Wireless Propag. Lett.*, vol. 17, no. 5, pp. 764–767, May 2018.

**ZHE WU** received the master's degree from Xidian University, in 2018, where he is currently pursuing the Ph.D. degree with the School of Electronic Engineering. His research interests include antenna design and object scattering characteristics of vortex electromagnetic waves.

**JIAJI WU** is currently a Professor and a Doctoral Supervisor with the School of Electronic Engineering, Xidian University. His research interests include natural image/hyperspectral image/aurora image/medical image compression coding, channel coding image transformation/classification/post-processing technology, and high-performance parallel computing.

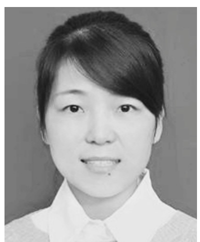

**TAN QU** received the bachelor's degree from Xidian University, in 2011, and the Ph.D. degree in physics, in 2016. In 2011, she studied for Ph.D. in radio physics without examination. From January 2017 to March 2017, she conducted postdoctoral research with Incheon National University, South Korea. In 2019, she was selected as a Master's Tutor. Her research interests include electromagnetic/optical wave transmission and scattering characteristics.

**ZHENSEN WU** (Senior Member, IEEE) received the B.Sc. degree in applied physics from Xi'an Jiaotong University, Xi'an, China, in 1969, and the M.Sc. degree in space physics from Wuhan University, Wuhan, China, in 1981. From 1995 to 2001, he was a Visiting Professor with Rouen University, Rouen, France, for implementing joint study of two projects supported by the Sino-France Program for Advanced Research. He is currently a Professor with Xidian University, Xi'an. His current research interests include electromagnetic and optical wave scattering and propagation in random media, computational electromagnetism, target and environment photoelectric characteristics, scattering properties from complex land-oceanic surface and remote sensing, electromagnetic wave propagation and modeling and prediction in troposphere and ionosphere, and high-performance computing. He is a fellow of the Chinese Institute of Electronics, Beijing, China.

**QIANG XU** was born in 1973. He received the bachelor's degree in applied physics from Sichuan University, in 1995, and the Ph.D. degree in optical engineering from Xidian University, in 2007. He has been teaching at Xidian University since he started his career. From January to June 2005 and from July 2013 to July 2014, he was a Visiting Student at the University of Illinois at Urbana–Champaign. He is currently an Associate Professor with the School of Physics and Optoelectronic Engineering, Xidian University. He is mainly engaged in the research of light transmission and scattering, photoelectric detection, optical remote sensing. He is a Senior Member of the Chinese Optical Society, a member of the Environmental Optical Committee, and a member of the Optical Engineering Society.

**HAIYING LI** received the B.S. degree in electronic information science and technology, and the Ph.D. degree in optics from Xidian University, Xi'an, China, in 2004 and 2009, respectively. Since 2011, she has been an Associate Professor with the School of Physics and Optoelectronic Engineering, Xidian University. From 2016 to 2017, she was a Visiting Scholar with the Department of Physics, Lancaster University, Lancaster, U.K. Her current research interest includes the propagation of electromagnetic wave in complex media.

**LIN YANG** graduated from Northwest Telecommunication Engineering College majoring in antenna, in 1983. From 1983 to January 2003, he worked at the Research Institute of Weapons Industry 206. In February 2003, he worked at the Institute of Antenna and Electromagnetic Scattering, Xidian University. His main research interests include antenna theory and engineering design.

**XIANGSHUAI MENG** was born in Liaocheng, Shandong, China, in August 1991. He received the B.S. degree from the Qingdao University of Technology, Qingdao, China, in 2014, and the Ph.D. degree without going through the conventional master's degree from Xidian University, Xi'an, China, in 2019. Since 2020, he has been with the School of Information and Communications Engineering, Xi'an Jiaotong University, and is currently an Assistant Professor. His recent research interests include reflectarray/transmitarray antennas, holographic surface impedance antennas, and electromagnetic vortex wave antennas.

**JING BAI** received the B.S. degree from Xidian University, in 2014, and the Ph.D. degree in physics, in 2019. Her research interests include target laser scattering characteristics, particle size analysis and measurement, and vortex beam propagation and its micromanipulation applications.